Ceramic nanocomposites prepared via the in situ formation of a novel TiZrN2 nanophase in a polymer-derived Si3N4 matrix

Mirna Chaker Bechelany, Abhijeet Lale, Maxime Balestrat, Christel Gervais, Sylvie Malo, Rafael Kenji Nishihora, Samuel Bernard

Ceramic nanocomposites prepared *via* the *in situ* formation of a novel $TiZrN_2$ nanophase in a polymer-derived Si_3N_4 matrix

Mirna Chaker Bechelany [a], Abhijeet Lale [b], Maxime Balestrat [b], Christel Gervais [c], Sylvie Malo [d], Rafael Kenji Nishihora [b,*], Samuel Bernard [b,*]

[a] Univ Lyo n, Université Claude Bernard Lyon 1, CNRS, Laboratoire des Multimatériaux et Interfaces, F-69622 Villeurbanne, France
[b] University of Limoges, CNRS, IRCER, UMR 7315, F-87000 Limoges, France
[c] Sorbonne Université, CNRS, Collège de France, Laboratoire Chimie de la Matière Condensée de Paris, 4 Place de Jussieu, 75005 Paris, France
[d] Laboratoire CRISMAT-ENSICAEN, Bd du Maréchal Juin,14050 Caen Cedex, France

ARTICLE INFO

Keywords:
Nanocomposites
Polymer-derived ceramics
Si_3N_4
$TiZrN_2$

ABSTRACT

The first demonstration of a nanoscaled titanium zirconium nitride ($TiZrN_2$) single-phase isolated during the preparation of polymer-derived silicon nitride (Si_3N_4) matrix nanocomposites is discussed. We employed a polysilazane, which was chemically modified with $Zr[N(CH_2CH_3)_2]_4$ and $Ti[N(CH_3)_2]_4$ then ammonolyzed before a pyrolysis step under ammonia (1000 °C) and a heat-treatment in flowing nitrogen (1000–1700 °C). Based on a careful control of the precursor chemistry in the early stage of the process and nano-/microstructural investigations of the material performed during its preparation, we were able to identify $TiZrN_2$ nanocrystals with a size as low as 9 nm distributed in α- and β-Si_3N_4 phases at a temperature as low as 1500 °C. We particularly proved that the $TiZrN_2$ nanophase could be generated because of the use of the polysilazane evoluting towards a covalently-bonded Si_3N_4 matrix . This unique nanostructure is expected to provide particular functionality to Si_3N_4 as noble metal-free catalysts and components with high plasmonic quality.

1. Introduction

Nitride materials have recently drawn a lot of interest in the field of high-tech ceramics due to their potential for energy-related applications [1–6]. Among the different families of nitrides, the fourth-column transition metal nitrides (TMN) such as titanium nitride (TiN) and zirconium nitride (ZrN) feature an unusual combination of outstanding properties such as electronic structure and high conductivity, resulting from their both metallic and covalent bonding characteristics [7]. They are particularly promising electrode materials suitable for a wide range of electrochemical energy storage devices. TiN, which has a metal-like conductivity with an outstanding chemical stability, has mostly been investigated as a platinum (Pt) support according to the fact that the TiN-Pt synergy can significantly enhance the activity and durability of the catalyst [8]. For oxygen reduction reactions in alkaline environ- ments, ZrN nanoparticles outperformed Pt deposited on a carbon sup- port [9]. Thus, the potential of TiN and ZrN in catalytic reactions involving energy-relevant transformations has substantially stimulated their proper design at nanoscale to enhance catalytic performance and to generate new physical phenomena [10].

The synthesis of TMNs as nanoparticles or nanostructured materials, on the other hand, is challenging due to the high temperatures required for preparation and the difficulties in controlling the particle size distribution. The polymer-derived ceramics (PDCs) route can tackle these issues by providing a way to *in situ* generating nanosized TMNs into a robust and covalently-bonded nitride matrix such as silicon nitride (Si_3N_4) [1,3,4,11–15]. Through a fundamental structure-property relationship, such TMN/Si_3N_4 nanocomposites can display totally new combinations of properties, especially by synergetic effect. As an illustration, this synthesis approach has recently provided a novel generation of TiN/Si_3N_4 nanocomposites as platinum (Pt) supports with unique properties for the complete and rapid dehydrogenation of $NaBH_4$ under alkaline conditions at 80 °C, owing to the synergetic effect between TiN and Pt nanoparticles [1]. More interestingly, the Si_3N_4 matrix demonstrated a catalytic activity, contributing to the system's exceptional performance. Within this context, we believe that combining in the same materials TiN and ZrN nanocrystals as well as Si_3N_4 using the PDCs route can provide a new generation of catalysts which does not require the

* Corresponding authors.
E-mail addresses: rafael.nishihora@hotmail.com (R.K. Nishihora), Samuel.bernard@unilim.fr (S. Bernard).

usage of noble metals.

Herein, we provide evidence of the identification of a novel nanoscaled TMN phase – a ternary $TiZrN_2$ nanophase with rock salt structure – isolated in a Si_3N_4 matrix through a fine control of both the chemistry in the early stage of the material design process – chemical modification step and ammonolysis – and the structural evolution of the material upon pyrolysis and high-temperature (HT) treatment (see Fig. 1). The evolutive process from the polymer to the final materials has been investigated in details.

2. Experimental part

2.1. Materials

The synthesis of the precursor is carried out in a purified argon atmosphere passing through a column of phosphorus pentoxide and then a vacuum/argon line by means of standard Schlenk techniques. The cleaned glassware is stored in an oven at 90 °C overnight before being connected to the vacuum/argon line, assembled and pumped under vacuum for 30 min and then filled with argon. All chemical products are

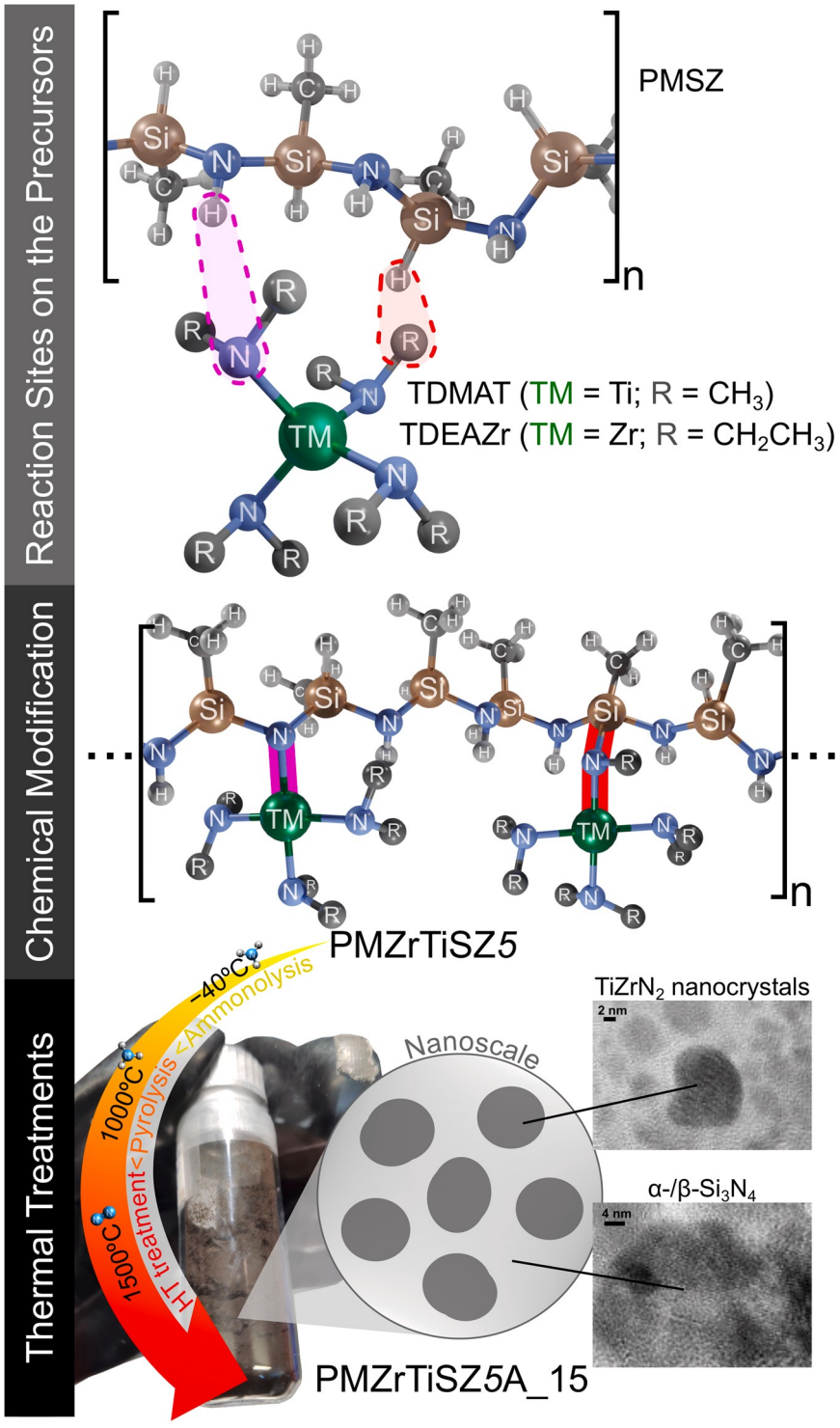

Fig. 1. Schematic diagram of the general process of designing $TiZrN_2/Si_3N_4$ nanocomposites from Ti and Zr-modified polysilazane.

handled in an argon-filled glove box (MBraun MB200B; O_2 and H_2O concentrations kept at < 0.1 ppm). Toluene (99.85%, Extra Dry over Molecular Sieve, AcroSeal(R)) was purchased from Acros Organics™. Dichloromethylsilane (DCMS) was obtained from Sigma-Aldrich and freshly distilled from magnesium at P_{atm} before use. Tetrakis(dimethylamino)titanium ($Ti[N(CH_3)_2]_4$, 99.99%) was obtained from Acros Organics™, stored in a fridge and used without further purification. It is labeled TDMAT. Tetrakis(diethylamino)zirconium ($Zr[N(CH_2CH_3)_2]_4$ (99%) was obtained from ABCR GmbH, stored in a fridge and used without further purification. It is labeled TDEAZr. Polymethysilazane (PMSZ) was synthesized by ammonolysis of DCMS ($HSiCH_3Cl_2$) in toluene according to procedures described in the literature [11,12] and served as a preformed polymer to form the nanocomposite precursor. FTIR of PMSZ (ATR/cm^{-1}): ν (N — H) = 3377 (m), ν (C—H) = 3040, (w), 2960 (s), 2860 (m), ν (Si—H) = 2105 (s), δ (CH_x) = 1458 (m) + 1406 (m), δ (Si—CH_3) = 1256 (s), δ (N-H): 1181 (m), δ (C-H + N — Si—N + Si-C) = 1005–630 (*vs*).

2.2. Synthesis of titanium and zirconium-modified polysilazanes

The reaction between PMSZ and TDEAZr and TDMAT has been performed at the temperature of reflux of toluene (115 °C) in a three-neck round-bottom flask. In a typical experiment, 1.57 g of TDEAZr (4.13 mmol) are firstly added with a syringe under argon atmosphere to a solution of 2.44 g of PMSZ (41.2 mmol referred to the monomeric unit of the polymer) in 80 mL of toluene at RT under vigorous stirring to directly form a yellow colored solution. Then, 0.93 g of TDMAT (4.15 mmol) are added according to the same procedure. When addition has ended, the temperature is increased up to 115 °C and kept at this temperature under vigorous stirring for three days. After cooling down, the solvent is extracted *via* an ether bridge (100 °C/1.5 • 10^{-1} mbar). The final products are collected inside the glove box to prevent air and moisture contact. The Zr- and Ti-modified PMSZ is labeled as **PMZrTiSZ*5*** (5 being the Si:(Zr+ Ti) ratio) as a powder. Anal. Found (wt %): Si 30.3, Ti 4.6, Zr 10.8, C 31.0, N 15.1, H 8.1, O 0.1. $[Si_{1.0}Ti_{0.1}Zr_{0.1}N_{1.0}C_{2.4}H_{7.5}]_n$ (*Referenced to* $Si_{1.0}$ and *oxygen content was omitted in the empirical formulae*). FTIR (KBr/cm^{-1}): ν(N — H) = 3377 (w), ν (C—H) = 2964 (s), 2865 (s), 2767 (s), ν(Si—H) = 2120 (*vs*), δ(CH_3) = 1458 (s), δ(CH_2) = 1364 (m), δ(C-N) = 1293 (s), δ(Si—CH_3) = 1252 (s), δ (N-H) 1180 (m), δ (C-H, N Si N, Si-C) 1174–655 (*vs*).

In a subsequent synthesis step, the as-synthesized polymer reacts with liquid ammonia to form a polymer labeled **PMZrTiSZ*5*A**: a solution of **PMZrTiSZ*5*** in 100 mL of toluene is introduced in three necks round bottom flask equipped with a reflux condenser and a gas inlet tube. The condenser and the flask are cooled down to −40 °C. Ammonia is introduced into the solution with a flow rate of 0.4 L min^{-1} until the saturation of the solution when a 2.5-fold excess of ammonia (referred to the amount of monomer units in the polymer) is reached. The mixture is kept 3 days before solvent elimination *via* an ether bridge (100 °C/ 1.5 • 10^{-1} mbar). The polymer labeled **PMZrTiSZ*5*A** was obtained as a yellow-orange powder. Anal. Found (wt%): Si 28.9, Ti 4.4, Zr 10.3, C 23.8, N 24.7, H 7.4, O 0.5. $[Si_{1.0}Ti_{0.1}Zr_{0.1}N_{1.8}C_{2.0}H_{7.4}]_n$ (*Referenced to* $Si_{1.0}$ and *oxygen content was omitted in the empirical formulae*). PMZrSZ*5*A and PMTiSZ*5*A samples have been prepared according to the same procedures to serve as references.

2.3. Preparation of the ceramic nanocomposites

Polymeric powders are placed in alumina boats in the glove-box, then introduced in a sealed tube under argon atmosphere to prevent any oxygen contamination of the samples during the transfer to the furnace. Powders are then introduced under argon flow into a silica tube inserted in a horizontal furnace (Nabertherm type RS 80/500/11, Ger- many). The tube is evacuated (0.1 mbar) and refilled with purified anhydrous ammonia (99.99%) to atmospheric pressure. Subsequently, the samples are subjected to a cycle of ramping of 5 °C•min^{-1} up to 1000 °C in flowing ammonia (dwelling time of 2 h at 1000 °C). A constant flow (120 mL min^{-1}) is passed through the tube during the pyrolysis cycle. After cooling under argon atmosphere, ammonia-pyrolyzed samples are stored in the glove-box for characterization. Samples are labeled **PMZrTiSZ*5*A_10** (according to the nature of the polymer), in which 10 refers to the two first digits of the temperature at which the polymer has been exposed. For the high temperature (T > 1000 °C) investigation, samples pyrolyzed at 1000 °C are subsequently introduced in a graphite furnace (Gero Model HTK 8) for HT treatments. The furnaces are pumped under vacuum (1• 10^{-1} mbar), refilled with nitrogen and maintained under a constant flow of gas (200 mL•min^{-1}) during the whole heat treatment. The program consists of a 5 °C.min^{-1} heating ramp up to the maximum temperature fixed in the range 1400–1700 °C, dwelling at the selected temperature for 2 h and cooling down to RT at 5 °C.min^{-1}. Samples are labeled PMZrTiSZ*5*A-T with T the two first digits of temperature (14, 15, 16 and 17) at which the material has been exposed (1400, 1500, 1600 and 1700 °C).

2.4. Material characterization

As the polymers are reactive towards moisture and oxygen, the following sample preparations are performed within a glove box. The chemical structure of polymers was determined by transmission FTIR spectroscopy using a Nicolet Magna 550 Fourier transform-infrared spectrometer. Solid-state ^{13}C CP MAS, ^{15}N CP MAS and ^{29}Si MAS NMR spectra were recorded on a Bruker AVANCE 300 spectrometer (7.0 T, $\nu_0(^1H)$ = 300.29 MHz, $\nu_0(^{13}C)$ = 75.51 MHz, $\nu_0(^{15}N)$ = 30.44 MHz, $\nu_0(^{29}Si)$ 59.66 MHz) using 4 mm and 7 mm Bruker probes and spin- ning frequencies of 10 and 5 kHz, respectively. ^{13}C and ^{15}N CP MAS experiments were recorded with ramped-amplitude cross-polarization in the ^1H channel to transfer magnetization from ^1H to ^{13}C and ^{15}N. (Recycle delay 3 s, CP contact time 1 ms, optimized ^1H spinal-64 decoupling). Single pulse ^{29}Si MAS NMR spectra were recorded with a recycle delay of 60 s. Chemical shift values were referenced to tetramethylsilane for ^{13}C and ^{29}Si and CH_3NO_2 for ^{15}N. Chemical analyses of the polymers were performed using a combination of several methods at Mikroanalytisches Labor Pascher (Remagen, Germany). Thermogravimetric analyses (TGA) of samples were performed in flowing ammonia at 5 °C •min^{-1} to 1000 °C using silica crucibles (Setaram TGA 92 16.18, SETARAM Instrumentation). The phase composition of ceramic samples was determined by XRD analysis (Bruker AXS D8 Discover, CuK_α radiation). The scans were performed in the range of 2θ 20°; 90° with a step of 0.015° and an exposure time of 0.7 s. The diffractograms were analyzed using the Diffrac.EVA software with the JCPDS-ICDD database. For Transmission electron Microscopy (TEM) study, as-prepared nanocomposite powders were crushed under n-butanol in an agate mortar and deposited the drops onto a holey carbon membrane supported by a copper grid. The Selected Area Electron diffraction (SAED) patterns and images were recorded, using a JEOL 2010 F microscope working at 300 kV.

3. Results and discussion

3.1. Polymer synthesis and structure

The foundation of the proposed approach is the synthesis of a pre-ceramic polymer - a solid compound labeled **PMZrTiSZ*5*** with a Si:(Zr+Ti) atomic ratio of 5 and displaying processability in solution and in the solid-state – from PMSZ which has been thoroughly characterized by FTIR, solid-state NMR (Fig. 2) and elemental analyses.

These characterization tools allowed demonstrating that **PMZrTiSZ*5*** is obtained *via* reactions already identified in the literature [11–14]:

(1) reactions between -NH units (*significant decrease of the FTIR bands assigned to N-H bonds at 3377 cm^{-1} (stretching) and at 1171 cm^{-1}*

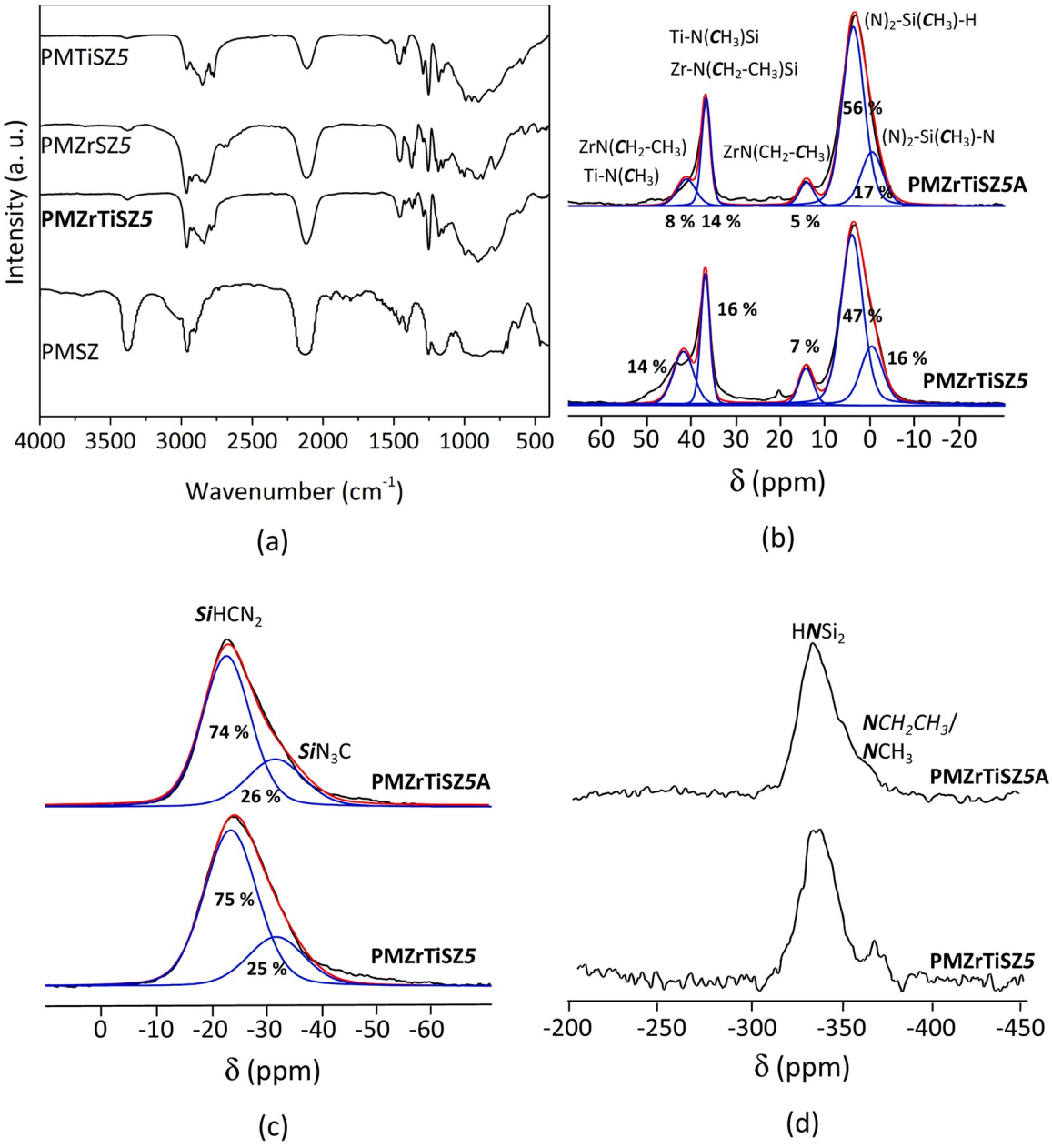

Fig. 2. FTIR spectrum recorded for the **PMZrTiSZ*5*** sample and compared to the FTIR spectra of PMSZ, PMZrSZ*5* and PMTiSZ*5* (a). Experimental and simulated ^{13}C CP MAS NMR (b), ^{29}Si MAS NMR (c) and ^{15}N CP MAS NMR (d) spectra recorded for the **PMZrTiSZ*5*** sample at 7 T.

(deformation), Fig. 2a) in PMSZ and -N(CH_2CH_3)$_2$/-N(CH_3)$_2$ groups in TDEAZr and TDMAT proceeded *via* release of diethylamine/dimethylamine to form -N-TM- (TM= Ti, Zr) bonds in **PMZrTiSZ*5*** (pink color, Fig. 1).

(2) reaction between the Si center of PMSZ and -N(CH_2CH_3)$_2$/-N(CH_3)$_2$ groups in TDEAZr and TDMAT (*low decrease of the FTIR band assigned to Si-H bonds at 2130 cm^{-1}*, Fig. 2a) with the concomitant evolution of ethane/methane to establish -Si-N(CH_2CH_3)-Zr- and/or -Si-N(CH_3)-Ti- bridges (*appearance of a set of broad bands in the range of 2865–2767 cm^{-1}* (Fig. 2a) *and presence of ^{13}C CP MAS NMR signals around 39 ppm* (Fig. 2b)) in the obtained precursor (red color, Fig. 1).

Based on the FTIR spectra of the PMTiSZ*5* and PMZrSZ*5* samples that serve as references, and the fairly low intensity of the Si-H band detected in the spectrum of the PMTiSZ*5* sample (with respect to the intensity of the Si-CH_3 band) compared to that one identified in PMZrSZ5, TDEAZr appeared to be less reactive toward SiH units than TDMAT. This is also visible in the spectrum of the **PMZrTiSZ*5*** sample. This can be explained by the -N(CH_2CH_3) units in TDEAZr that provide a higher steric hindrance compared to -NCH_3 units in TDMAT. As a result, it should generate a polymer, **PMZrTiSZ*5***, with a degree of crosslinking intermediate between the PMTiSZ*5* and PMZrSZ*5* samples. In this regard, we proposed that **PMZrTiSZ*5*** sample's crosslinking degree be increased by ammonia reaction at low temperature [11]. Thus, **PMZrTiSZ*5*** was reacted with a 2.5-fold excess of ammonia (based on the amount of monomer units in the polymer) at 40 °C for three days under stirring before being allowed to warm to 25 °C and distilled, generating a sample labeled **PMZrTiSZ*5*A**.

Elemental analyses of the latter ($[Si_{1.0}Ti_{0.1}Zr_{0.1}N_{1.8}C_{2.0}H_{7.4}]_n$, the oxygen content was < 2 at% and could be neglected) showed that the Si:Zr and Si:Ti ratios calculated in **PMZrTiSZ*5*** ($[Si_{1.0}Ti_{0.1}Zr_{0.1}N_{1.0}C_{2.4}H_{7.5}]_n$, the oxygen content was < 2 at% and could be neglected) are sustained in **PMZrTiSZ*5*A** whereas carbon and

nitrogen contents changed: the comparison of the chemical compositions clearly indicated that nitrogen is introduced by reaction with ammonia and that carbon is removed during this process. This inherently affects the carbon and nitrogen environment in the polymer as observed by solid-state NMR.

The ^{13}C CP MAS NMR spectrum of **PMZrTiSZ*5*A** (Fig. 2b) exhibited three main signals around 3, 15 and 40 ppm, which were assigned based on our previous works [11–14] and common to those identified in the ^{13}C NMR spectrum of **PMZrTiSZ*5***. It emphasizes that ammonolysis mainly affects the intensities of the signals attributed to Zr-N(CH_2***C***H_3) (15 ppm) and Ti-N(***C***H_3)/Zr-N(***C***H_2CH_3) (40 ppm) units (compared to the intensity of the signal attributed to Si***C***H_3 environments around 3 ppm) without affecting the chemical environment of the silicon atoms in the polymer. We hypothesized that terminal —N(CH_2CH_3)$_2$/-N(CH_3)$_2$ groups are preferentially replaced by NH_2 units, which may further condensate to form -NH- bridges linking Si and/or Ti elements. Therefore, the crosslinking degree (formation of bridges) and reactivity (formation of NH units) of the **PMZrTiSZ*5*A** sample are increased, both of which are pre-requisites to limit the weight loss during the polymer-to-ceramic conversion. Accordingly, the ^{29}Si MAS spectra of both samples are analogous (Fig. 2c). They exhibit a main broad line, which can be fitted with two overlapping signals, *i.e.* resonances of CH_3-***Si***(H)N_2 units at 23 ppm and CH_3-***Si***N_3 environments at around –31 ppm based on our previous works [16–18]. The solid-state ^{15}N CP MAS NMR spectrum of **PMZrTiSZ*5*A** (Fig. 2d) shows a broadened signal centered at —335 ppm. The signal around —365 ppm in the spectrum of **PMZrTiSZ*5***, which has been ascribed to -***N***CH_2CH_3/-***N***CH_3 sites [19], is significantly reduced in the **PMZrTiSZ*5*A** spectrum. This confirms the ammonia's reactivity toward -NR_2 units (R = CH_3, CH_2CH_3) *via* amine exchange reactions.

The mechanisms described above allow establishing Ti-N and Zr-N bonds in the polysilazanes (in addition to already present Si-N bonds) that are prerequisite to form the TiN and ZrN nanophases within Si_3N_4.

3.2. *Polymer-to-ceramic conversion*

The thermo-chemical conversion of the **PMZrTiSZ*5*A** sample has been monitored by thermogravimetric analysis (TGA) in an ammonia atmosphere (Fig. 3).

The TG curve of the **PMZrTiSZ*5*A** sample displays a three-step weight loss in the temperature range 25 1000 °C, *i.e.*, from 25° to 250°C (1st weight loss), from 250° to 600°C (2nd weight loss) and from 600° to 1000°C (3rd weight loss). At 1000 °C, a final weight loss of 27% is measured, although the profile of the curve shows that the thermochemical transformation is not fully achieved at this temperature. This is most probably related to the continuous release of hydrogen in the sample above 1000 °C, which is generally observed in PDCs even after a pyrolysis at 1000 °C [20]. As expected, the weight loss recorded up to 1000 °C in the **PMZrTiSZ*5*A** sample is less pronounced than in the **PMZrTiSZ*5*** sample. This is due to the former's higher degree of crosslinking and the presence of a greater portion of groups (*e.g.*, NH/NH_2) in its structure that are able to react together (or with other groups such as residual SiH units) during the pyrolysis. After the pyrolysis step, X-ray diffraction revealed that the **PMZrTiSZ*5*A_10** sample is fully amorphous as shown by the presence of a flat pattern (Fig. 4). Thus, **PMZrTiSZ*5*A_10** was subsequently heat-treated under nitrogen at 1400–1700 °C in order to evaluate its high-temperature behavior with respect to crystallization, phase separation and microstructure evolution.

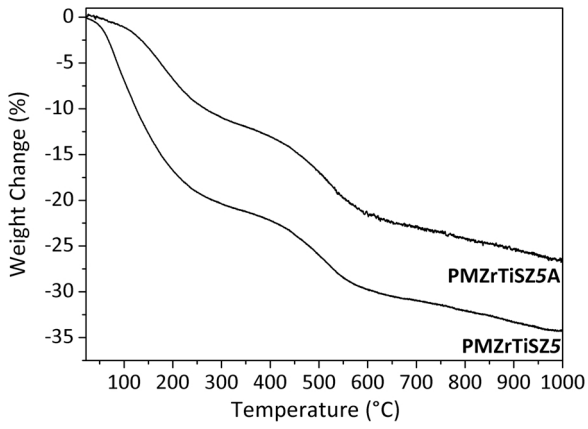

Fig. 3. TG curves recorded during decomposition of the **PMZrTiSZ*5*A** and **PMZrTiSZ*5*** samples in flowing ammonia.

3.3. *High temperature behavior of the amorphous single-phase ceramics*

Fig. 4 compares the XRD pattern of the **PMZrTiSZ*5*A_10** sample with those of the samples isolated in the temperature range 1400 °C (**PMZrTiSZ*5*A_14**) – 1700 °C (**PMZrTiSZ*5*A_17**).

The XRD pattern of the **PMZrTiSZ*5*A_14** sample ($Si_{1.0}Ti_{0.2}Zr_{0.2}N_{1.5}$ as measured by EDS) revealed better defined peaks at 2θ 35.7°, 41.8°, and 60.6° although still quite broad, indicating a very small crystallite size of about 1.81 nm, which was calculated at the dominant (111) peak. Although the peak positions are fairly far apart, we tentatively suggested that the XRD patterns exhibit the (111), (200), and (311) peaks from the rock salt TiN (ICDD PDF 00-038-1420) and ZrN (ICDD PDF number: 04-004-2860) phases in the cubic Fm-3 m space group. After heat-treatment at 1500 °C, the XRD pattern of the **PMZrTiSZ*5*A_15** sample ($Si_{3.0}Ti_{0.7}Zr_{0.8}N_{5.0}$ as measured by EDS) identified a substantial crystallization of the material (crystallite size 15 nm) and displayed typical XRD peaks of a rock-salt TMN structure at 34.8°, 40.3°, 58.4°, 69.8°, 73.3°, and 87.5°, with peak positions still quite different from the rock salt TiN and ZrN phases. HT treatment at 1500 °C also induced crystallization of α (ICDD PDF number: 04-005-5074) and β (ICDD PDF number: 04-033-1160) -Si_3N_4. In order to elucidate the structure of the TMN phase formed at 1500 °C, we firstly compared the XRD pattern of the **PMZrTiSZ*5*A_15** sample with those of the PMZrSZ*5*A_15 (prepared from PMZrSZ*5*A) and PMTiSZ*5*A_15 (prepared from PMTiSZ*5*A) samples obtained following the same polymer synthesis, pyrolysis, and HT treatment (Fig. 5). We showed clear evidence that the former displays TMN peak positions that differ from those identified in the XRD patterns for the PMZrSZ*5*A_15 and PMTiSZ*5*A_15 samples. In PMZrSZ*5*A_15, a ZrN phase is identified by the dominant peaks at 34.0° (111), 39.4° (200), 56.9° (220), 68° (311), 71.4° (222), and 84.7° (400), along the peaks characteristic of the α and β phases of Si_3N_4. The most pronounced crystallinity of the Si_3N_4 phase in PMZrSZ*5*A_15 compared to the

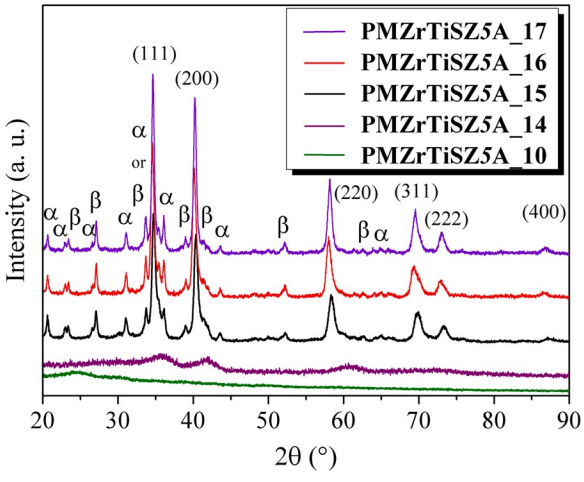

Fig. 4. X-ray patterns of **PMZrTiSZ*5*A_10**, **PMZrTiSZ*5*A_14**, **PMZrTiSZ*5*A_15**, **PMZrTiSZ*5*A_16** and **PMZrTiSZ*5*A_17**.

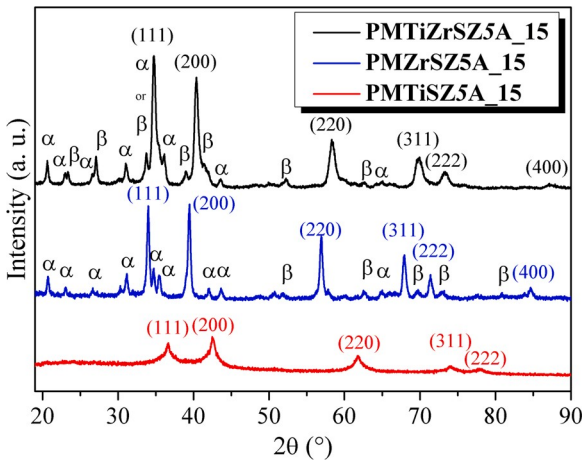

Fig. 5. Comparison of the X-ray patterns of **PMZrTiSZ5A_15**, PMZrSZ5A_15 and PMTiSZ5A_15.

PMTiSZ5A_15, which only reported the TiN nanophase identified by the broad peaks at 36.6° (111), 42.6° (200), 61.9° (220), 74.1° (311), and 77.8° (222), is related to the lowest TMN content in the former (because of the lower reactivity of TDEAZr toward – at least – Si-H bonds of PMSZ during the PMTiSZ5 synthesis) compared to the latter, as we already demonstrated in the Si-Ti-N systems by varying the Si:Ti ratio [13].

Secondly, we compared the XRD pattern of the **PMZrTiSZ5A_15** sample to that of the TiNZrN_15 material, which was formed from a mixture of TDEAZr and TDMAT (Zr:Ti ratio of 1) and therefore without PMSZ, using the same synthesis, pyrolysis, and HT procedure (Fig. 6).

Again, the XRD pattern of TiNZrN_15 is noticeably different: it showed the diffraction peaks of both highly crystallized TiN and ZrN nanophases and - because of the great sensitivity of the precursors to air and moisture, it identified an oxynitride phase. Hence, this tends to demonstrate the key role of the precursor which evolved upon heat-treatment towards a Si_3N_4 matrix in the formation of the $TiZrN_2$ phase.

According to Ref. [21], fcc titanium and zirconium nitrides are completely miscible at 2000 K. Later studies by *ab initio* calculations predicted critical temperatures of the miscibility gap in the δ phase of TiN-ZrN system changing from 1880 K [22] (x_{ZrN} = 0.35) to 5000 K [23] (x_{ZrN} 0.36). More recently, Kumar et al. predicted *via ab initio* calculations a critical temperature and composition of miscibility gap of 1844 K and 0.34 (x_{ZrN}), respectively [24].

Based on our results and the referenced computation-aided material design approaches, we can highlight the nanoconfinement effect provided by the PDC matrix toward the formation of the nanosized $TiZrN_2$

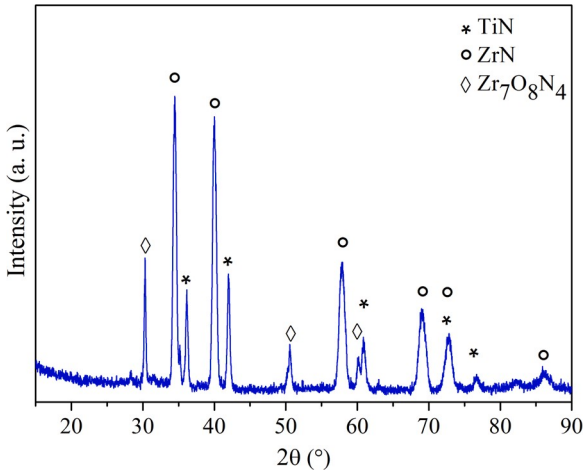

Fig. 6. X-ray pattern of TiNZrN_15.

phase in the **PMZrTiSZ5A_15** sample at relatively low temperature: the reducing properties of the polysilazane coupled with the formation of a covalently-bonded Si_3N_4 matrix most probably trigger the formation of the rock salt $TiZrN_2$ (ICDD PDF number: 01-077-3008) nanophase (and retain its nanoscale size)– identified by the presence of the XRD peak at 2θ 34.8° [25] in the XRD pattern of the **PMZrTiSZ5A_15** sample – at much lower temperature than expected by thermodynamic predictions and observed without the presence of Si_3N_4 matrix (Fig. 6). The isolation of this $TiZrN_2$ phase was confirmed through the continuous increase of the high-temperature treatment of the **PMZrTiSZ5A_15** sample at 1600 °C (**PMZrTiSZ5A_16**) and 1700 °C (**PMZrTiSZ5A_17**). Heat-treatments confirmed the extended crystallization of the different constitutive phases, as evidenced by sharper and more intense $TiZrN_2$ peaks along with XRD peaks (Fig. 4) of α- and β-Si_3N_4 in the XRD pattern of the **PMZrTiSZ5A_16** sample ($Si_{1.0}Ti_{0.2}Zr_{0.2}N_{1.6}$ as measured by EDS; $TiZrN_2$ crystallite size = 19.8 nm) and of the **PMZrTiSZ5A_17** sample ($Si_{1.0}Ti_{0.2}Zr_{0.2}N_{1.7}$ as measured by EDS; $TiZrN_2$ crystallite size = 22.4 nm).

TEM examinations were carried out on the sample in which the $TiZrN_2$ phase has been identified at the lowest temperature, *i.e.*, **PMZrTiSZ5A_15** sample, to obtain micro- and nanostructural information related to the nanocomposite (Fig. 7). The majority of the nanocrystals in the **PMZrTiSZ5A_15** sample are oriented in the (111) crystallographic direction, according to HRTEM measurements. Furthermore, Fig. 7a associated with the SAED pattern indicated a significant extent of the crystallization in the **PMZrTiSZ5A_15** sample. In particular, the distinct rings in the SAED pattern could be indexed to the (hkl) planes of silicon and transition metal nitride phases. We could clearly observe the presence of nanocrystals (Fig. 7a,b) with the lattice spacings typical of the $TiZrN_2$ (Fig. 7c) and Si_3N_4 (Fig. 7d) phases. The inset of Fig. 7c - corresponding to the HRTEM image recorded on an [111] oriented $TiZrN_2$ nanoparticle with the calculated image surrounded by a superimposed yellow rectangle (thickness 50 Å and Δf = 550 Å) - evidenced a good matching between the calculated and experimental images; thereby validating the cubic structural model. As an illustration, the corresponding FFT image as an insert in Fig. 7d indicated the crystallization of the matrix in the α phase.

Thus, HRTEM findings are consistent with the XRD results, demonstrating the formation of a nanocomposite made of nanosized $TiZrN_2$ crystals scattered in a crystallized Si_3N_4 matrix. A particle size distribution was generated from a series of low-magnification TEM images, showing an average particle size of 9 nm with a standard deviation of 5 nm, indicating that it remains distributed over a relatively large range of diameter (See Fig. 1SI in ESI) at the nanoscale. This unique nanostructural feature of the nanocomposites is expected to provide particular functionality to Si_3N_4 – not only as noble metal-free catalysts – but also for instance as hard materials as well as components with high plasmonic quality [26]. This functionality is under investigation and will be presented in a separated paper.

4. Conclusion

In conclusion, the reaction of tetrakis-(dimethylamino)titanium ($Ti[N(CH_3)_2]_4$) and tetrakis(diethylamino)zirconium ($Zr[N(CH_2CH_3)_2]_4$) with polymethylsilazane (PMSZ) in toluene in a combined 1:5 at. (Ti Zr:Si) ratio generated a Ti- and Zr-modified PMSZ. These samples were subsequently ammonolyzed and heat-treated in flowing ammonia up to 1000 °C then in nitrogen up to 1500 °C to favor the *in-situ* growth of nanoscaled rock salt $TiZrN_2$ phase in a silicon nitride matrix. The highlights can be summarized as follows:

(1) Formation of a *single-source* precursor by the reaction of $Ti[N(CH_3)_2]_4$ and $Zr[N(CH_2CH_3)_2]_4$ with the Si center and NH groups of PMSZ at toluene reflux.
(2) The rock salt $TiZrN_2$ phase grew within the surrounding Si_3N_4 matrix in the temperature range 1000–1500 °C.

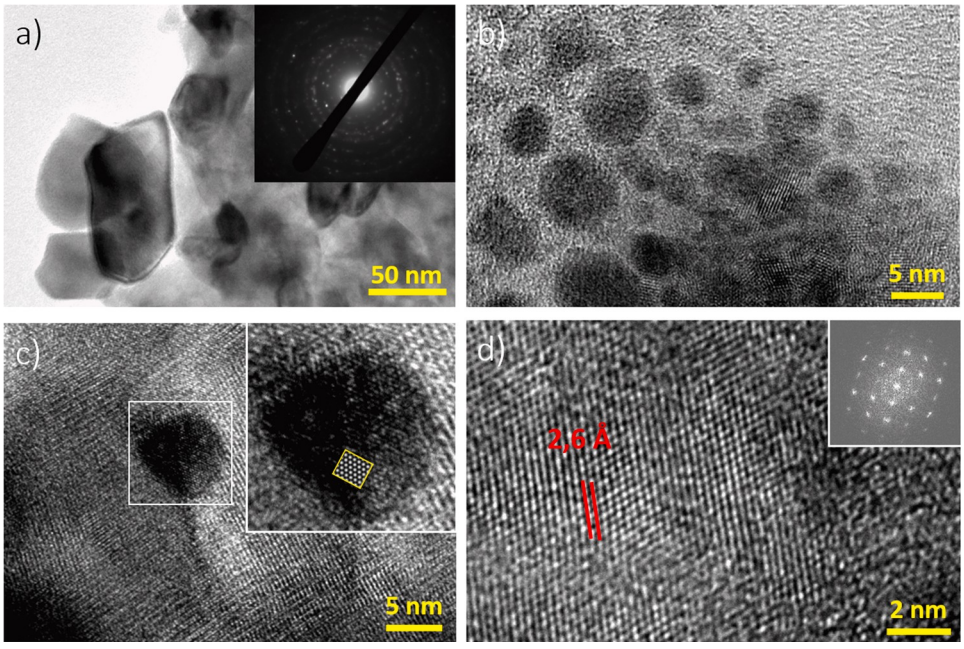

Fig. 7. HRTEM images of **PMZrTiSZ5A_15** (a–d).

(3) The reducing properties of the polysilazane coupled with the formation of a covalently-bonded silicon nitride matrix upon heating - triggered the growth of the $TiZrN_2$ phase at a temperature as low as 1500 °C and allowed maintaining the $TiZrN_2$ particle size as nanoscale.

This study paves the way for the design of nanoscaled TMNs in nanocomposites, which may be applied in a wide range of applications. This is expected to lead to several structural and functional applications for a new generation of advanced ceramics.

Declaration of Competing Interest

The authors declare that they have no known competing financial interests or personal relationships that could have appeared to influence the work reported in this paper.

Acknowledgements

Authors thank the French Rhône-Alpes Council (Cible 2010 project – Contract n°1897-"Nanocomposites multifonctionnels pour applications microtechniques, horlogères et joaillères"). Dr. Samuel Bernard acknowledge the funding agency Agence Nationale de la Recherche (ANR) through the Carapass project (Project number ANR-16-CE08-0026) and the Indo-French Centre for the Promotion of Advanced Research (CEFIPRA, Project No. 5108-1) for providing financial support for the Ph.D. Maxime Balestrat and the postdoc fellows of Abhijeet Lale.

References

[1] A. Lale, M.D. Mallmann, S. Tada, A. Bruma, S. Özkar, R. Kumar, M. Haneda, R. A. Francisco Machado, Y. Iwamoto, U.B. Demirci, S. Bernard, Appl. Catal. B Environ. 272 (2020), 118975.
[2] A. Lale, S. Bernard, U.B. Demirci, ChemPlusChem 83 (2018) 893.
[3] I. AlShibane, J.S. Hargreaves, A.L. Hector, W. Levason, A. McFarlane, Dalton Trans. 46 (2017) 8782.
[4] C. Zhou, A. Ott, R. Ishikawa, Y. Ikuhara, R. Riedel, E. Ionescu, J. Eur. Ceram. Soc. 40 (2020) 6280–6287.
[5] A. Zakutayev, J. Mater. Chem. A 4 (2016) 6742.
[6] R. Han, F. Liu, X. Wang, M. Huang, W. Li, Y. Yamauchi, X. Sun, Z. Huang, J. Mater. Chem. A 8 (2020) 14384.
[7] S.T. Oyama, in: S.T. Oyama (Ed.), The Chemistry of Transition Metal Carbides and Nitrides, Springer, Berlin, Germany, 1996.
[8] H. Nan, D. Dang, X.L. Tian, J. Mater. Chem. A 6 (2018) 6065.
[9] Y. Yuan, J. Wang, S. Adimi, H. Shen, T. Thomas, R. Ma, J.P. Attfield, M. Yang, Nat. Mater. 19 (2020) 282.
[10] A.B. Dongil, Nanomaterials 9 (2019) 1111.
[11] M.C. Bechelany, V. Proust, C. Gervais, R. Ghisleni, S. Bernard, P. Miele, Adv. Mater. 26 (2014) 6548.
[12] M.C. Bechelany, V. Proust, A. Lale, P. Miele, S. Malo, C. Gervais, S. Bernard, Chem. Eur. J. 23 (2017) 832.
[13] A. Lale, V. Proust, M.C. Bechelany, A. Viard, S. Malo, S. Bernard, J. Eur. Ceram. Soc. 37 (2017) 5167.
[14] M. Balestrat, A. Lale, A.V.A. Bezerra, V. Proust, E.W. Awin, R.A.F. Machado, P. Carles, R. Kumar, C. Gervais, S. Bernard, Molecules 25 (2020) 5236.
[15] C. Zhou, X. Gao, Y. Xu, G. Buntkowsky, Y. Ikuhara, R. Riedel, E. Ionescu, J. Eur. Ceram. Soc. 35 (2015) 2007.
[16] L. Gottardo, S. Bernard, C. Gervais, K. Inzenhofer, G. Motz, M. Weinmann, C. Balan, P. Miele, J. Mater. Chem. 22 (2012) 7739.
[17] A. Viard, L. Gottardo, D. Lopez-Ferber, A. Soleilhavoup, C. Salameh, S. Samal, Y. Gueguen, T. Rouxel, G. Motz, F. Babonneau, C. Gervais, S. Bernard, Dalton Trans. 46 (2017) 13510.
[18] A. Viard, D. Fonblanc, M. Schmidt, A. Lale, C. Salameh, A. Soleilhavoup, M. Wynn, P. Champagne, S. Cerneaux, F. Babonneau, G. Chollon, F. Rossignol, C. Gervais, S. Bernard, Chem. Eur. J. 23 (2017) 9076.
[19] D. Fonblanc, D. Lopez-Ferber, M. Wynn, A. Lale, A. Soleilhavoup, A. Leriche, Y. Iwamoto, F. Rossignol, C. Gervais, S. Bernard, Dalton Trans. 47 (2018) 14580.
[20] M. Balestrat, E. Diz Acosta, O. Hanzel, N. Tessier-Doyen, R. Machado, P. Šajgalík, Z. Lenčéš, S. Bernard, J. Eur. Ceram. Soc. 40 (2020) 2604.
[21] P. Duwez, F. Odell, J. Electrochem. Soc. 97 (1950) 299.
[22] A. Wang, S.-L. Shang, Y. Du, L. Chen, J. Wang, Z.-K. Liu, J. Mater. Sci. 47 (2012) 7621.
[23] A. Hörling, J. Sjölén, H. Willmann, T. Larsson, M. Odén, L. Hultman, Thin Solid Films 516 (2008) 6421.
[24] S. Sridar, R. Kumar, K.C. Hari Kumar, Calphad 56 (2017) 102.
[25] G. Pradhaban, P. Kuppusami, D. Ramachandran, K. Viswanathan, R. Ramaseshan, Mater. Today Proc. 3 (2016) 1627.
[26] L. Chen, Y. Ran, Z. Jiang, Y. Li, Z. Wang, Nanomaterials 10 (2020) 829.